Journal of Traditional and Complementary Medicine 14 (2024) 598–610

Contents lists available at ScienceDirect

Journal of Traditional and Complementary Medicine

journal homepage: www.elsevier.com/locate/jtcme

In vivo evaluation of *Andrographis paniculata* and *Boesenbergia rotunda* extract activity against SARS-CoV-2 Delta variant in Golden Syrian hamsters: Potential herbal alternative for COVID-19 treatment

Supasek Kongsomros [a,1], Tussapon Boonyarattanasoonthorn [a,1], Wallaya Phongphaew [b], Chaiyan Kasorndorkbua [b], Piyanate Sunyakumthorn [c], Rawiwan Im-Erbsin [c], Luis A. Lugo-Roman [c], Teetat Kongratanapasert [d], Jiraporn Paha [e], Suwimon Manopwisedjaroen [e], Pakakrong Kwankhao [f], Kittitach Supannapan [f], Nittaya Ngamkhae [f], Nitipol Srimongkolpithak [g], Pornpun Vivithanaporn [a], Suradej Hongeng [h], Arunee Thitithanyanont [e,**], Phisit Khemawoot [a,*]

[a] *Chakri Naruebodindra Medical Institute, Faculty of Medicine Ramathibodi Hospital, Mahidol University, Samutprakarn, 10540, Thailand*
[b] *Department of Pathology, Faculty of Veterinary Medicine, Kasetsart University, Bangkok, 10900, Thailand*
[c] *Department of Veterinary Medicine, United States Army Medical Directorate, Armed Forces Research Institute of Medical Sciences (USAMD-AFRIMS), Bangkok, 10400, Thailand*
[d] *Program in Translational Medicine, Faculty of Medicine Ramathibodi Hospital, Mahidol University, Bangkok, 10400, Thailand*
[e] *Department of Microbiology, Faculty of Science, Mahidol University, Bangkok, Thailand*
[f] *Chao Phya Abhaibhubejhr Hospital Foundation, Prachinburi, 25000, Thailand*
[g] *National Center for Genetic Engineering and Biotechnology (BIOTEC), National Science and Technology Development Agency (NSTDA), Pathum Thani, 12120, Thailand*
[h] *Department of Pediatrics, Faculty of Medicine Ramathibodi Hospital, Mahidol University, Bangkok, 10400, Thailand*

ARTICLE INFO

Keywords:
Andrographis paniculata
Zingiberaceae
SARS-CoV-2
Golden Syrian hamsters
COVID-19

ABSTRACT

The ongoing COVID-19 pandemic has triggered extensive research, mainly focused on identifying effective therapeutic agents, specifically those targeting highly pathogenic SARS-CoV-2 variants. This study aimed to investigate the *in vivo* antiviral efficacy and anti-inflammatory activity of herbal extracts derived from *Andrographis paniculata* and *Boesenbergia rotunda*, using a Golden Syrian hamster model infected with Delta, a representative variant associated with severe COVID-19. Hamsters were intranasally inoculated with the SARS-CoV-2 Delta variant and orally administered either vehicle control, *B. rotunda*, or *A. paniculata* extract at a dosage of 1000 mg/kg/day. Euthanasia was conducted on days 1, 3, and 7 post-inoculation, with 4 animals per group. The results demonstrated that oral administration of *A. paniculata* extract significantly alleviated both lethality and infection severity compared with the vehicle control and *B. rotunda* extract. However, neither extract exhibited direct antiviral activity in terms of reducing viral load in the lungs. Nonetheless, *A. paniculata* extract treatment significantly reduced IL-6 protein levels in the lung tissue (7278 ± 868.4 pg/g tissue) compared to the control (12,495 ± 1118 pg/g tissue), indicating there was a decrease in local inflammation. This finding is evidenced by the ability of *A. paniculata* extract to reduce histological lesions in the lungs of infected hamsters. Furthermore, both extracts significantly decreased IL-6 and IP-10 mRNA expression in peripheral blood mononuclear cells of infected hamsters compared to the control group, suggesting systemic anti-inflammatory effects occurred. In conclusion, *A. paniculata* extract's potential therapeutic application for SARS-CoV-2 arises from its observed capacity to lessen inflammatory cytokine concentrations and mitigate lung pathology.

Peer review under responsibility of The Center for Food and Biomolecules, National Taiwan University.

* Corresponding author. Chakri Naruebodindra Medical Institute, Faculty of Medicine Ramathibodi Hospital, Mahidol University, Bang Phli, Samut Prakarn, 10540, Thailand.

** Corresponding author. Department of Microbiology, Faculty of Science, Mahidol University, Bangkok, 10400, Thailand.

E-mail addresses: arunee.thi@mahidol.edu (A. Thitithanyanont), phisit.khe@mahidol.ac.th (P. Khemawoot).

[1] Contributed equally.

https://doi.org/10.1016/j.jtcme.2024.05.004
Received 23 October 2023; Received in revised form 8 May 2024; Accepted 15 May 2024
Available online 16 May 2024

List of abbreviations

ALI	Acute lung injury
ALT	Alanine aminotransferase
BSL-3	Biosafety level 3
DMEM	Dulbecco's Modified Eagle's Medium,
FFA	Focus forming assay
FFU	Focus forming units
H&E	Hematoxylin and eosin
IFN-γ	Interferon-gamma
IL-1β	Interleukin-1β
IL-6	Interleukin-6
IL-6R	Interleukin-6 receptor
IP-10	Interferon-gamma-induced protein 10
ISH	In situ hybridization
LCMS	Liquid chromatography-mass spectrometry
LLOQ	Lower limit of quantification
MEM	Minimum essential medium
MIP-1α, -1β	Macrophage inflammatory protein 1α and 1β
PBMCs	Peripheral blood mononuclear cells
PBS	Phosphate buffered saline
PFU	Plaque forming units
SARS-CoV-2	Severe acute respiratory syndrome coronavirus 2
TNF	Tumor necrosis factor
VEGF	Vascular endothelial growth factor
VOC	Variants of concern

1. Introduction

The COVID-19 pandemic caused by the severe acute respiratory syndrome coronavirus 2 (SARS-CoV-2) continues to pose a significant threat to public health worldwide.[1] As of April 14, 2024, COVID-19 has affected approximately 775 million people worldwide, resulting in up to 7.0 million fatalities (https://covid19.who.int). Efforts to develop SARS-CoV-2 vaccines have effectively reduced COVID-19 mortality and morbidity and contributed significantly to controlling the global pandemic.[2] However, the emergence of new variants raises concerns regarding the efficacy of the vaccines because these variants possess the ability to evade neutralizing antibodies developed post-vaccination.[3] Given the pandemic's urgency, the repurposing of antivirals like remdesivir, molnupiravir, and ritonavir-nirmatrelvir (Paxlovid) has been instrumental in expediting therapeutics. These FDA emergency approved drugs effectively inhibit a wide spectrum of SARS-CoV-2 variants and hold promise in reducing COVID-19's progression.[4,5] Alternatively, it is recommended that hospitalized COVID-19 patients receive immunomodulators such as corticosteroids, and interleukin-6 receptor (IL-6R) blockers (e.g., tocilizumab or sarilumab), to prevent cytokine storms in severe cases of COVID-19.[6–8] Despite progress in COVID-19 treatments, maintaining diverse therapeutic options is crucial considering the issues surrounding vaccination inadequacies, antiviral limitations, drug resistance, supply shortages, and accessibility.[9–11] Herbal medicines rich in bioactive compounds[12,13] have demonstrated potential efficacy against COVID-19. Notably, our earlier research revealed the anti-SARS-CoV-2 properties of *Andrographis paniculata*[14] and *Boesenbergia rotunda*[15] in cell culture. *B. rotunda*, known for its diverse bioactive compounds, has antiviral, antibacterial, and anti-inflammatory properties,[16–20] and previous studies demonstrated that it reduced lung inflammation in infected hamsters.[21] *A. paniculata*, a Southeast Asian native herb,[22] exhibits anti-inflammatory, antiviral, antioxidant, and hepatoprotective effects,[22–27] mainly by suppressing pro-inflammatory cytokines via the NF-κB and MAPK pathways[28–30]; its primary bioactive compound, andrographolide, has broad antiviral properties.[31] Both *A. paniculata* extract and andrographolide showed *in vitro* antiviral activity against SARS-CoV-2 and inhibited SARS-CoV-2's Mpro activity.[14,32,33] Given the shortages of antiviral treatment and vaccines, Thailand's Ministry of Public Health authorized the use of *A. paniculata* extracts, commonly known as "Fah Talai Jone" for treating mild COVID-19 symptoms.[34] However, despite ongoing studies on its real-world effectiveness,[35] solid evidence supporting its use as a COVID-19 treatment is limited, emphasizing the need for more preclinical and clinical studies. COVID-19 is transitioning from an international emergency to an enduring health issue[36] and we are facing complexities in therapeutic development due to the emergence of new variants, which complicate the path to effective treatments.[37,38] While the current circulating variant Omicron typically causes milder symptoms and requires less intensive care,[39] the Delta variant, which was dominant in late August 2021,[40] poses the greatest pathogenic threat and is associated with severe disease risk and high hospitalization rates.[41–44] Delta's high fusogenicity, which causes syncytial formation, and its dependence on TMPRSS2 for entry increase its pathogenicity.[45–50] In contrast, Omicron forms fewer syncytia, indicating it is less reliant on TMPRSS2 and potentially has a less severe disease course.[51–53] Nevertheless, Omicron's high mutation rate and the introduction of specific substitutions (L452R, R346T, N460K, V83A) in its subvariants heighten its fusogenicity, generating concerns about possible increases in disease severity.[54,55] These substitutions may contribute to increased virulence and more severe disease. Additionally, the severity of COVID-19 is strongly associated with the excessive release of proinflammatory cytokines, known as hypercytokinemia or cytokine storm, which can lead to multiple organ failure.[56–59] Patients with severe COVID-19 exhibit a more pronounced cytokine storm, characterized by elevated levels of various cytokines such as interleukin-1β (IL-1β), interleukin-6 (IL-6), interferon-gamma-induced protein 10 (IP-10), tumor necrosis factor (TNF), interferon-gamma (IFN-γ), macrophage inflammatory protein 1α and 1β (MIP-1α, -1β), and vascular endothelial growth factor (VEGF).[58] Among these cytokines, IL-6 is a key mediator of the inflammatory response of severe COVID-19 [60]. Elevated IL-6 levels are associated with disease progression and respiratory failure and can be used as a marker for monitoring severe COVID-19 patients.[60] For these reasons, our focus was on studying the Delta variant because this warrants prioritization in preclinical trials, to potentially guide effective strategies against future, similarly virulent, variants. Therefore, the objective of our study was to assess the efficacy of *A. paniculata* and *B. rotunda* extracts as antiviral agents and their ability to reduce inflammation in Golden Syrian hamsters infected with the SARS-CoV-2 Delta variant. We examined several parameters, including survival rate, body weight loss, clinical symptoms, lung viral load, cytokine levels, and lung histology, in hamsters treated with the extracts compared to a control group. Our findings contribute to understanding the therapeutic benefits of *A. paniculata* and *B. rotunda*, highlighting their potential efficacy as alternative therapeutic strategies against COVID-19.

2. Materials and methods

2.1. Cells

TMPRSS2-expressing VeroE6 cell lines (Vero E6/TMPRSS2 cells) were obtained from the Japanese Collection of Research Bioresources (JCRB) Cell Bank, Japan (JCRB number: JCRB1819). TMPRSS2, a surface-localized protease, is responsible for cleaving and activating the SARS-CoV-2 spike protein, essential for viral entry into host cells.[61] The cells were cultured in Dulbecco's Modified Eagle's Medium (DMEM) with low glucose (Gibco, USA), supplemented with 10 % heat-inactivated FBS (Gibco), 1 mg/mL of G418 (Nacalai Tesque,

Japan), and 100 U/mL penicillin–streptomycin (Gibco). A human ACE2-and TMPRSS2-expressing A549 lung carcinoma cell line (A549-hACE2-TMPRSS2) (a549-hace2tpsa) was obtained from InvivoGen. Cells were cultured in high-glucose DMEM supplemented with 10 % heat-inactivated FBS, 2 mM L-glutamine, 100 U/mL penicillin–streptomycin, 100 μg/mL normocin (Invivogen), 0.5 μg/mL puromycin (Invivogen), and 300 μg/mL hygromycin B (Invivogen). Vero cells (ATCC: CCL-81) were grown in minimum essential medium (MEM) supplemented with 10 % heat-inactivated FBS and 100 U/mL penicillin–streptomycin. DMEM and MEM were used to supply essential nutrients and maintain an optimal environment for each cell culture. All cell lines were incubated at 37 °C in an incubator containing 5 % CO_2.

2.2. Viruses

SARS-CoV-2 variants were isolated from a patient who had been admitted to a hospital in Thailand and tested positive for COVID-19 via real-time PCR. The Delta variant (SARS-CoV-2/human/THA/NH657_P3/2021; Accession number: MZ815438), Alpha variant (SARS-CoV-2/human/THA/NH088_P3/2021; Accession number: MZ815440.1), and Omicron BA.2.10 variant (SARS-CoV-2/human/THA/OTV114/2022) were used in this study. To propagate the virus, Vero E6/TMPRSS2 cells were cultured in low-glucose DMEM supplemented with 2 % FBS, 100 U/mL penicillin, 1 mg/mL of G418, and 100 μg/mL streptomycin. After 96 h of incubation at 37 °C in a 5 % CO_2 incubator, the infected cells were harvested for viral titer determination by plaque assay. All experiments involving the SARS-CoV-2 virus were conducted in a certified Biosafety level 3 (BSL-3) laboratory located at the Department of Microbiology, Faculty of Science, Mahidol University, Thailand.

2.3. Plaque assay

Vero cells were used for performing the standard plaque assay. Briefly, 10-fold serial dilutions of the SARS-CoV-2 viruses were grown on the Vero cells for 1 h, and subsequently, the supernatant was removed and the cells overlaid with plaque assay medium. The medium contained a final concentration of 1.2 % Avicel (RC581; FMC BioPolymer, USA), 2 % FBS (Gibco), 100 U/mL penicillin (Gibco), and 100 μg/mL streptomycin (Gibco). At 3 d.p.i., the cells were fixed with 3.7 % formaldehyde for 1 h before the overlay medium was removed, and the cells were stained in 1.25 % crystal violet solution. The plaques were counted and the plaque-forming units (PFU)/mL calculated.

2.4. Extracts and reagents

The herb extracts were provided by the Chao Phya Abhaibhubejhr Hospital Foundation Under the Royal Patronage of H.R.H. Princess Bejraratanarajsuda, Thailand. *B. rotunda* extract was obtained using CO_2 extraction and found to contain 29.0 % w/w of panduratin A (Supplementary Table 1). *A. paniculata* extract was prepared by 95 % ethanol extraction and had 14.24 % w/w of andrographolide (Supplementary Table 2). For analysis, puerarin as internal standard (purity >98 %) and andrographolide (purity >95 %) were purchased from Sigma-Aldrich, USA. The analytical standard for panduratin A (purity >98 %) was supplied by Biosynth Carbosynth, UK.

2.5. Animal experiment and ethics statement

Male, 8-week-old, Golden Syrian Hamsters were purchased from Charles River Laboratories, Inc. The animals were randomly divided into experimental groups and kept for 7 days in a temperature-controlled room (20–22 °C) with 12:12 h light/dark cycles for quarantine and acclimatization. Their health status was checked by measuring their alanine aminotransferase (ALT) and creatinine levels prior to starting the experiment. The animals were group-housed in an HEPA-filtered cage system and were provided with commercial diet and chlorinated water *ad libitum*. A total of 36 hamsters were divided into three groups ($n = 12$ per group) to receive 2 mL/kg/day dimethyl sulfoxide (DMSO as vehicle control), 1000 mg/kg/day *A. paniculata* extract, or 1000 mg/kg/day *B. rotunda* extract with loading dose 1000 mg/kg on the first day. All hamsters were anesthetized by isoflurane, and 25 μL of SAR-CoV-2 (dose 5×10^4 PFU) were dropped into each nostril with a pipette in a total volume of 50 μL. At 12 h post-inoculation, the hamsters were administered the vehicle control, *B. rotunda* extract, or *A. paniculata* extract (oral administration, p.o.) twice-daily (BID, 12 h intervals) with a maintenance dose of 500 mg/kg for 7 consecutive days. The virus inoculum and extract dosages were selected in accordance with established *in vivo* study on the prototypical SARS-CoV-2 strain.[21] This foundational work verified the susceptibility of the model to the virus, ensuring reliable disease development, and also established the safety and therapeutic efficacy of the extract treatments. A schematic of the experimental design for therapeutic treatment of the hamster model is shown in Fig. 1A. Animals ($n = 4$) from each group were euthanized after receiving the test compound 4 h after infection on days 1, 3, 7. To align our examination timings corresponding with the pre-symptomatic, symptomatic, and recovery stages of infection observed in hamsters stages with human infection Specifically, 12 h post-infection in hamsters corresponds to 1–3.5 days in humans, representing the pre-symptomatic stage; 3 days post-infection in hamsters aligns with the symptomatic stage in humans; and 7 days post-infection in hamsters matches the recovery stage. This model was utilized to simulate the timely administration of herbal extracts early in human infection.[62,63] Blood and lung tissues were collected at necropsy for further analysis. A humane endpoint was applied when the animals exhibited severe clinical signs (Supplementary Table 3) along with body weight reduction of more than 15 % from their initial body weight. All animal work under the protocol number 21-08 was reviewed and approved by the Institutional Animal Care and Use Committee of the Armed Forces Research Institute of Medical Sciences (AFRIMS), Bangkok, Thailand (Approval date: July 26, 2021). The facility is fully accredited by AAALAC International, and all animal work was performed in compliance with the ARRIVE guidelines. All procedures involving SARS-CoV-2 were performed in a certified animal biosafety level 3 laboratory at the Department of Veterinary Medicine, AFRIMS, Bangkok.

2.6. Focus forming assay

To quantify the infectious titers of SARS-CoV-2, homogenized lung tissues were processed using focus forming assay (FFA). In brief, 10-fold serial dilutions of tissue supernatants were added to Vero cells in 96-well plates for 60 min. After carefully removing the inoculum from the cell monolayer, DMEM medium, which contained 1.2 % Avicel (RC581; FMC BioPolymer, USA), 2 % FBS (Gibco), 100 U/mL penicillin (Gibco), and 100 μg/mL streptomycin (Gibco), was added. The plates were kept in a 5 % CO_2 incubator at 37 °C for 24 h. The medium was removed and replaced with 4 % formaldehyde in phosphate buffered saline (PBS) for 60 min to fix the cell monolayer, then washed three times with PBS. For viral foci detection, the cells were permeabilized in 0.5 % triton X-100 at room temperature for 10 min. After that, we washed the cells twice in PBS, and a 1:2500 dilution of rabbit monoclonal antibody against SARS-CoV-2 Nucleoprotein (Sino Biological, China) was added, and the cells incubated at room temperature for 60 min. The cells were washed three times with PBS, and a 1:1000 dilution of horseradish peroxidase-conjugated goat anti-rabbit IgG secondary antibody (Dako, USA) was added, followed by incubation. Then True-Blue peroxidase substrate (Sera Care, USA) was applied to stain the cells. Viral foci were counted, and we evaluated the viral load in the lung tissue in terms of focus forming units (FFU) per gram of tissue.

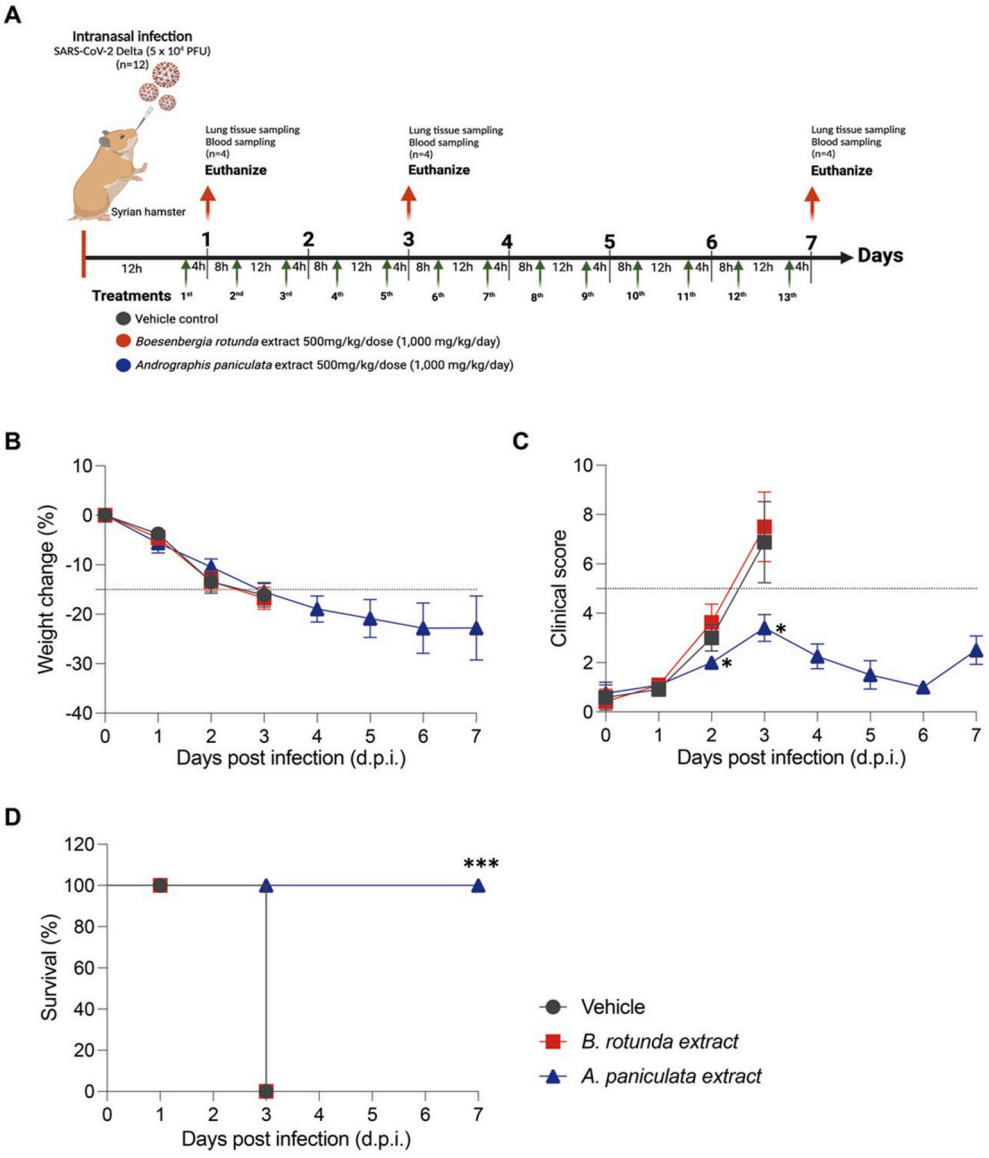

Fig. 1. Therapeutic effects of *A. paniculata* and *B. rotunda* extracts on SARS-CoV-2 infected hamsters: weight change, clinical observation, and survival analysis. (A) Schematic of the experimental design for therapeutic treatment in a hamster model. Golden Syrian hamsters were inoculated with 5×10^4 PFU of SARS-CoV-2 Delta variant. Vehicle control (DMSO at 2 mL/kg/day), *A. paniculata* extract (1000 mg/kg/day), or *B. rotunda* extract (1000 mg/kg/day) was administered orally 12 h after inoculation. Treatment was then continued every 12 h for 7 consecutive days until end of the experiment. Hamsters were daily monitored for body weight change (B), clinical observation (C) and survival (D) for 7 days. The data are presented as mean ± SD. Statistical analysis was performed by using non-parametric Kruskal-Wallis test with Dunn's multiple testing. *$p < 0.05$, ***$p < 0.001$.

2.7. IL-6 detection

To the homogenized lung tissues was added 10X RIPA lysis buffer (ab156034, Abcam, UK) to achieve 1 × concentration to inactivate SARS-CoV-2. The samples were incubated at room temperature for 45 min and then diluted 1:5 with DMEM media. IL-6 concentrations (pg/mL) were measured in the lung tissue using individual ELISA kits for IL-6 (MBS700950, MyBioSource, USA) following the manufacturer's instructions.

2.8. IL-6, IP-10, and TNFα mRNA expression

Total RNA was extracted from homogenized lung tissue and peripheral blood mononuclear cells (PBMCs) using the RNeasy Mini kit (Qiagen, Germany), and gene expression levels were assessed by real-time quantitative reverse transcription PCR (qRT-PCR) using the One-Step RT-PCR kit (Qiagen). Primer pairs for hamster β-actin, IL-6, IP-10, and TNF-α genes were chosen from a previously published study[64] as follows: Hamster ACTB primer 1 (5′-GGC CAG GTC ATC ACC ATT-3′); Hamster ACTB primer 2 (5′-GAG TTG AAT GTA GTT TCG TGG ATG-3′); Hamster IL-6 primer 1 (5′-GGT ATG CTA AGG CAC AGC ACA CT-3′); Hamster IL-6 primer 2 (5′-CCT GAA AGC ACT TGA AGA ATT CC-3′); Hamster IP-10 primer 1 (5′-GCC ATT CAT CCA CAG TTG ACA-3′); Hamster IP-10 primer 2 (5′-CAT GGT GCT GAC AGT GGA GTC T-3′); Hamster TNF-α primer 1 (5′-AGC TGG TTG TCT TTG AGA GAC ATG-3′); Hamster TNF-α primer 2 (5′-GGA GTG GCT GAG CCA TCG T-3′). The qRT-PCR conditions consisted of incubation at 60 °C for 30 min, 95 °C for 15 min, followed by 40 cycles of 95 °C for 30 s, 55 °C for 30 s, and 72 °C for 30 s. Using Rotor Gene Q software (Qiagen), standard curves were generated for the viral spike RNA using a known concentration of SARS-CoV-2 RNA for absolute viral gene quantification, expressed as gene copies/g tissue. The ΔΔCT method was employed to calculate the relative cytokine expression levels, which were then normalized to β-actin mRNA and reported as relative expression levels compared to the

vehicle control group.

2.9. Determination of panduratin A and andrographolide concentration in the plasma and lung tissue

All herbal extracts were freshly prepared in DMSO and administered to the infected animals every 12 h after inoculation, which continued for 7 consecutive days. The experimental groups ($n = 12$ per group) in this study consisted of vehicle, *B. rotunda* extract, and *A. paniculata* extract groups. The extracts were administered with a loading dose of 1000 mg/kg and a maintenance dose of 500 mg/kg BID for 7 consecutive days. Venous blood and lung tissue samples were collected 4 h after administration on days 1, 3, and 7. Blood samples were centrifuged at 5000×*g* for 5 min to obtain the plasma and kept at −20 °C until analysis. Lung tissues were mixed with 2.8-mm stainless-steel beads (Benchmark Scientific, USA) operated using a BeadBug bead homogenizer at 3000 rpm for 3 min. The mixtures were then centrifuged at 5000×*g* for 5 min to obtain supernatant and kept at −20 °C. The bioactive compounds of the *B. rotunda* and *A. paniculata* extracts (panduratin A and andrographolide) were determined by LCMS method. Bioanalytical validation was conducted in compliance with USFDA guidance, and the results are shown in Supplementary Table 4. Fifty microliters of the biological samples were transferred to 200 μL of acetonitrile, which contained puerarin (20 ng) as the internal standard (IS). The mixtures were vortexed for 10 min and then centrifuged at 12,000×*g* for 10 min at 4 °C to obtain the supernatant. Ten microliters of the supernatants were directly injected into the LCMS system.

2.10. Instruments and analytical conditions

The LCMS analyses were carried out with an ExionLC Series equipped with QTRAP 4500 triple quadrupole mass spectrometer (AB Sciex, USA). In the stationary phase, a Synergi Fusion-RP C18 column (Phenomenex, USA) was used for chromatographic separation and the temperature in the column was maintained at 35 °C. The gradient system of the mobile phase was composed of 0.1 % formic acid in water (A) and acetonitrile (B) and run in accordance with the following conditions. (A) was run at 90 % over 0.0–0.5 min, 90%–10 % over 0.5–3.0 min, 10 % over 3.0–4.5 min, and 10%–90 % over 4.5–6.0 min, and maintained at 90 % for 1.5 min as the initial condition at a flow rate of 0.4 mL/min. Quantification was obtained using multiple reaction monitoring in negative mode of the transition at a mass to charge of 405.2/166.0 for panduratin A, at a mass to charge of 395.2/330.7 for andrographolide, and at a mass to charge of 415.0/294.9 for puerarin (IS). The bioanalytical validation method for the targeted analytes was adopted from our previous published paper because it showed good specificity and linearity for all of the targeted analytes and IS. The calibration curves were linear over the selected concentration range in different matrices with a coefficient of determination $R^2 > 0.99$. The concentration range of andrographolide was within the range of 10–10,000 μg/L while panduratin A was within the range of 1–1000 μg/L. All compounds in this study showed a lower limit of quantification (LLOQ) within the range of 1–10 μg/L. Analytical software version 1.7.1 and MultiQuant software version 3.0.3 (AB Sciex, USA) were used for data acquisition and evaluation. The chromatograms, retention times, and chemical structures of the target analytes in solvent and plasma are shown in Supplementary Figs. 1, 2, and 3, respectively.

2.11. Lung histopathology

Necropsy of the lung tissues was conducted in the ABSL3 laboratory. In brief, lung tissues were fixed in 10 % neutral buffered formalin for a minimum of 48 h, and then tissues were embedded in paraffin. Embedded tissues were sectioned at 4 μm and dried overnight at 40–42 °C before staining. The tissue sections were processed for Hematoxylin and Eosin (H&E) staining using a series of xylene substitutes and isopropanol for de-paraffinization and rehydration before dying. The stained sections were sent for lesion evaluation by board-certified veterinary pathologists.

2.12. In situ hybridization for SARS-CoV-2 RNA detection

In situ hybridization (ISH) was performed using the RNAscope 2.5 HD Red Detection Kit (Advanced Cell Diagnostics, USA) according to the manufacturer's instructions. The V-nCoV2019-S RNAscope probe (Advanced Cell Diagnostics) specific for the SARS-CoV-2 S gene based on isolate Wuhan-Hu-1 (Genbank accession number, NC_045512.2, targeting region 21631–23303) was used. Briefly, formalin-fixed paraffin-embedded lung tissue sections were de-paraffinized. Tissue sections were then pre-treated with H_2O_2 for 10 min at room temperature, and 1 × target retrieval solution was added for 15 min in a steamer that maintained the temperature above 99 °C. The sections were transferred to be incubated with Protease Plus (Advanced Cell Diagnostics) for 30 min at 40 °C and then incubated with the SARS-CoV-2-specific probe for 2 h at 40 °C in a HybEZ oven (Advanced Cell Diagnostics). A Fast Red solution was used for detecting the signal, and the stained sections were counterstained with 50 % Gill hematoxylin III (Sigma Aldrich) for 2 min. The final sections were sent for lesion evaluation by board-certified veterinary pathologists.

2.13. Acute lung injury scoring system

H&E-stained sections were evaluated for the severity of lung damage by two independent pathologists using the acute lung score (ALI) scoring system from the American Thoracic Society.[65] Five independent variables related to histological evidence of injury were adopted as follows: (A) the presence of neutrophils in the alveolar space, (B) the presence of neutrophils in the interstitial space, (C) the formation of hyaline membranes, (D) the presence of proteinaceous debris in the airspaces, and (E) thickening of the alveolar septum. The injury score was within the range of 0–1, which was calculated using the equation, ALI score = ((20 × A) + (14 × B) + (7 × C) + (7 × D) + (2 × E))/(number of fields × 100).

2.14. Statistical analysis

All statistical tests were performed using GraphPad Prism version 5 (GraphPad Company). The Kaplan-Meier Survival with Log-rank Test was used to measure the difference of the survival outcomes, and the Kruskal-Wallis Test with Dunn's Multiple Test was selected for determine the differences of other outcomes. P value of <0.05 was considered statistically significant.

3. Results

3.1. Administration of therapeutic A. paniculata extract alleviates the lethality and clinical signs caused by SARS-CoV-2 Delta infection in Golden Syrian hamsters

In our recent study, we demonstrated the promising *in vitro* anti-SARS-CoV-2 activities of *A. paniculata* extract and its bioactive compound andrographolide, as well as *B. rotunda* extract and its phytoconstituent panduratin A. Both andrographolide and panduratin A exhibited post-infection anti-SARS-CoV-2 activity on human airway epithelial cells (Calu-3).[14,15] Extending these finding, we accessed the *in vivo* antiviral efficacy of these two extracts using a Golden Syrian hamster model, which is well-established for efficacy studies with the prototypic SARS-CoV-2 (Wuhan strain).[21] We used the SARS-CoV-2 Delta variant for our investigation which is known for its ability to induce severe disease in the hamsters and its high viral replication, pathogenicity, and transmissibility compared with the prototypic SARS-CoV-2.[46,66,67] Before conducting the experiment, we acclimatized the hamsters and monitored their health by measuring serum ALT and creatinine levels to

assess liver and kidney functions, which were found to be within normal ranges (Supplementary Table 5). Golden Syrian hamsters were intranasally inoculated with 5×10^4 PFU of the SARS-CoV-2 Delta variant. At 12 h post-inoculation, the hamsters were administered the vehicle control, *B. rotunda* extract, or *A. paniculata* extract (oral administration, p.o.) twice-daily (BID, 12 h intervals) with a loading dose of 1000 mg/kg (first dose) and a maintenance dose of 500 mg/kg for 7 days (Fig. 1A). Body weight changes and clinical observations were monitored daily. Viral loads, cytokines, and histopathological changes in the lungs were determined to evaluate the *in vivo* efficacy of the extracts. Infected hamsters were euthanized when they lost more than 15 % body weight and exhibited severe clinical signs (clinical score ≥5) according to the daily clinical observation record/score sheet (Supplementary Table 3). The results showed that, at 1 day post-infection (d.p.i.), none of the infected hamsters showed significant weight loss or severe clinical signs (Fig. 1B and C). However, at 3 d.p.i., most infected hamsters in the vehicle control (n = 8) and *B. rotunda* extract (n = 8) groups exhibited euthanasia criteria due to severe clinical signs, such as ruffled fur, hunched posture, ocular discharge, panting, or rapid breathing (total clinical signs score ≥5) and a progressive weight loss of 15 % (Fig. 1B and C). In contrast, infected hamsters receiving *A. paniculata* extract had a significantly lower clinical score compared with the vehicle control group at 2 d.p.i. and 3 d.p.i. and survived until 7 d.p.i. (Fig. 1C), resulting in a 100 % survival rate (Fig. 1D). These findings indicate that *A. paniculata* extract offer more effective protection against the SARS-CoV-2 Delta variant in hamsters compared with *B. rotunda* extract and vehicle control.

3.2. Concentrations of panduratin A and andrographolide in plasma and lung tissues of infected hamsters administered B. rotunda and A. paniculata extracts

In a parallel experiment using LCMS, we determined the concentrations of panduratin A and andrographolide in the plasma and lung tissues of hamsters infected with SARS-CoV-2 Delta and treated with *A. paniculata* and *B. rotunda* extracts. The results presented in Table 1 demonstrate that the levels of panduratin A in the plasma of infected hamsters receiving *B. rotunda* extract at a dosage of 1000 mg/kg/day were approximately 4.21 μM at 1 d.p.i. and 7.27 μM at 3 d.p.i. These concentrations were 2- to 3.6-times higher than the IC_{50} of panduratin A observed in an *in vitro* model of SARS-CoV-2 (2.04 μM). Similarly, the plasma concentrations of andrographolide in hamsters treated with *A. paniculata* extract at 1000 mg/kg/day p.o. were approximately 5.48 μM at 1 d.p.i., 5.51 μM at 3 d.p.i., and 8.01 μM at 7 d.p.i. (Table 1). These concentrations were 3.3- to 4.7-fold higher than the average IC_{50} (1.68 μM) used for inhibiting SARS-CoV-2 in Calu-3 cells.[14] However, we observed lower concentrations of panduratin A and andrographolide in the lung tissue compared to the plasma. The average concentrations of panduratin A and andrographolide in lung tissue were approximately 0.19–0.26 μg/g and 0.75–0.80 μg/g, respectively (Table 1). On the basis of the estimated water content of lung tissue, which is approximately 80 % by weight,[68] the calculated concentrations of panduratin A in the lung tissue were 0.37 μM at 1 d.p.i. and 0.52 μM at 3 d.p.i. (Table 1), which were lower than the *in vitro* IC_{50} observed in Calu-3 cells.[15] The estimated concentrations of andrographolide in the lung tissue were 1.72 μM and 1.83 μM for 1 d.p.i. and 3 d.p.i., respectively, which were slightly higher than the average IC_{50} value found in Calu-3 cells.[14] The calculated lung-to-plasma (L/P) ratio of andrographolide was approximately 0.3–0.4, while that of panduratin A was around 0.1, indicating there was limited penetration of the compound into the lungs.

Table 1
The concentration of Panduratin A and Andrographolide in plasma and lung tissues of the infected hamsters.

Type of samples	Experimental groups		
	Vehicle	*B. rotunda* extract 1000 mg/kg p.o.	*A. paniculata* extract 1000 mg/kg p.o.
		Panduratin A	Andrographolide
Plasma (μg/L)			
Day 1	ND	1710.4 ± 284.3 (~4.21 μM)	1921.3 ± 508.4 (~5.48 μM)
Day 3	ND	2954.1 ± 582.1 (~7.27 μM)	1930.1 ± 257.7 (~5.51 μM)
Day 7	ND	N/A	2808.1 ± 547.4 (~8.01 μM)
Lung (μg/g)			
Day 1	ND	0.186 ± 0.015 (~0.37 μM)	0.750 ± 0.206 (~1.72 μM)
Day 3	ND	0.262 ± 0.047 (~0.52 μM)	0.800 ± 0.144 (~1.83 μM)
Day 7	ND	N/A	0.850 ± 0.181 (~1.94 μM)

ND: not detected; N/A: not available. The data are presented as mean ± SD, (n = 12 per experimental group, n = 4 per subgroup).

3.3. Therapeutic B. rotunda and A. paniculata extracts do not affect viral load in the lungs of SARS-CoV-2-infected hamsters

The significant finding that *A. paniculata* extract reduced the severity and lethality of SARS-CoV-2 infection in hamsters, despite the limited penetration of the bioactive compounds of *B. rotunda* and *A. paniculata* extracts into the lung tissues, inspired further investigations. In these, we aimed to evaluate the antiviral efficacy of both extracts against SARS-CoV-2 in Golden Syrian hamsters. We determined the infectious viral titers in the lung homogenates of infected hamsters treated with the extracts using a FFA. The viral titers were calculated as FFU per gram of tissue. All infected hamsters that reached the euthanasia criteria at 3 d.p.i. were included in the analysis. Lung infectious titers at 3 d.p.i. were not significantly reduced in the *B. rotunda* (n = 8) or *A. paniculata* (n = 4) extract-treated groups compared to the vehicle control group (n = 8) (Fig. 2A). Additionally, we determined the viral RNA load in the lungs of SARS-CoV-2-infected hamsters using qRT-PCR with primers targeting the spike gene. The viral RNA load was expressed as RNA copies per gram of lung tissue for each hamster. The results showed that lung RNA loads were not significantly reduced in the *B. rotunda* (n = 8) or *A. paniculata* (n = 4) extract-treated groups compared with the vehicle control group (n = 8) (Fig. 2B). We also conducted *in situ* hybridization to detect the presence of viral infection in the lungs of hamsters at 3 d.p.i. by staining lung tissue sections for SARS-CoV-2 spike RNA. No significant reduction in spike RNA was observed in the lungs of hamsters treated with *B. rotunda* or *A. paniculata* extracts compared with those of the control group (Fig. 2C and D). The results demonstrated that neither *B. rotunda* nor *A. paniculata* extracts significantly lowered viral load or spike RNA levels in the lungs of hamsters infected with SARS-CoV-2

3.4. Therapeutic A. paniculata extract, but not B. rotunda, significantly reduces IL-6 in the lung tissue of infected hamsters

Previous studies have shown that elevated levels of inflammatory cytokines, including IL-1β, IL-6, IP-10, TNFα, interferon-γ, MIP-1α/1β, and VEGF, are associated with the severity and complications of COVID-19 [56-59], with increased IL-6 levels strongly linked to lower survival rates.[60] Our recent findings demonstrated that *A. paniculata* extract improved survival among SARS-CoV-2-infected hamsters without reducing viral loads in the lung, indicating potential anti-inflammatory benefits that could improve lung pathology. To better understand the efficacy of *A. paniculata* and *B. rotunda* extracts in modulating the inflammatory response, we further evaluated their impact on cytokine levels, focusing on IL-6 as a representative cytokine, as well as assessing the mRNA expression levels of cytokines IL-6, IP-10, and TNFα. Lung tissues were harvested at 3 d.p.i., and then subjected to homogenization. We determined the IL-6 concentration in lung tissue homogenates using an ELISA kit specific for hamster IL-6. The results showed that treatment with *A. paniculata* extract (n = 4) significantly reduced the IL-6 levels in

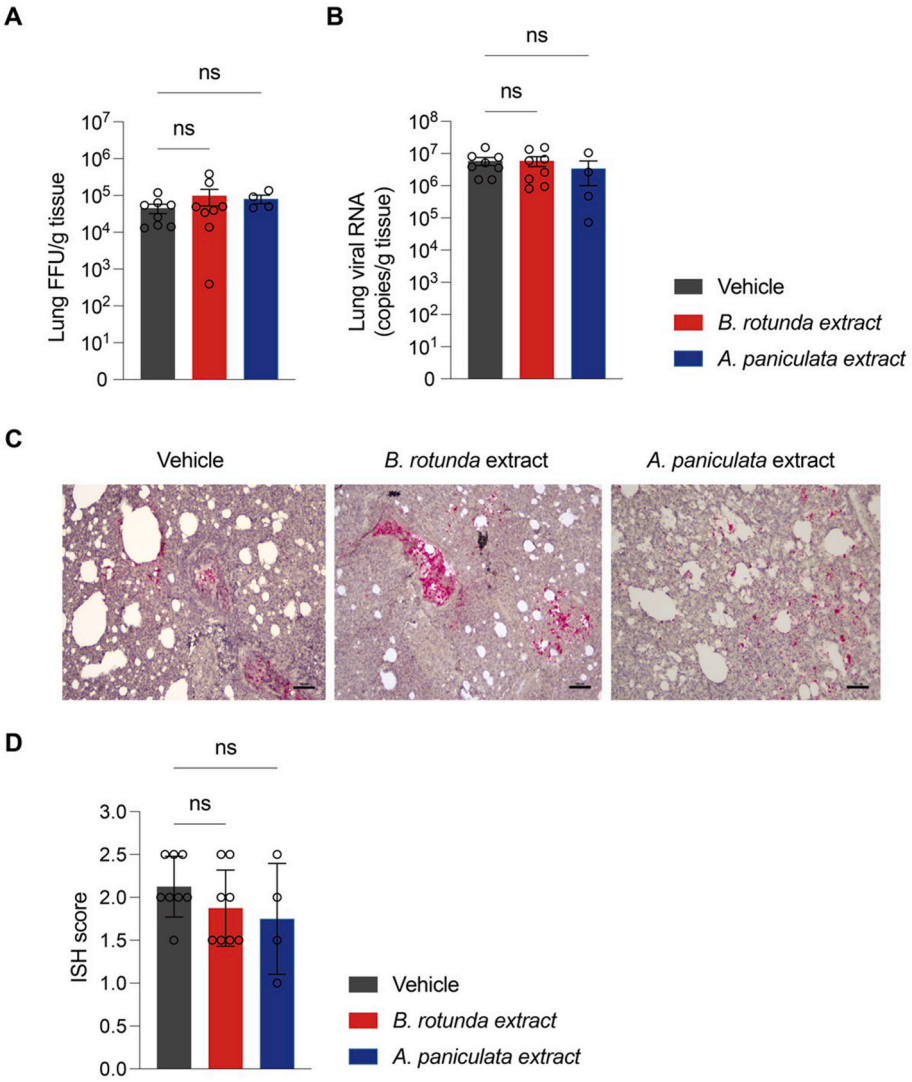

Fig. 2. Infectious viral titer, RNA load, and *in situ* hybridization analysis of SARS-CoV-2 infected hamsters treated with *B. rotunda* or *A. paniculata* extracts. (A) Infectious viral titer in the lungs of SARS-CoV-2 infected hamsters in vehicle control, *B. rotunda* or *A. paniculata* extract-treated groups was determined by focus forming assay at 3 days post-infection (d.p.i.). (B) Viral RNA load in lung tissues were determined by qRT-PCR targeting the spike RNA at 3 d.p.i. (C) Representative figures of *in situ* hybridization (ISH) for the detection of SARS-CoV-2 RNA targeting spike (S) gene in the lung autopsy tissue sections of each group at 3 d.p.i. Scale bar: 50 μm. (D) ISH score of the lung of infected hamster treated with the extracts compared to the vehicle control group is shown. The data are presented as mean ± SEM (A and B), mean ± SD (D) from 4 to 8 hamster per group. Each dot represents individual hamster. Statistical analysis was performed by using non-parametric Kruskal-Wallis test with Dunn's multiple testing. ns, not significant.

the lung tissue induced by SARS-CoV-2 (7278 ± 868.4 pg/g tissue) compared with the vehicle control group (n = 8) at 3 d.p.i. (12,495 ± 1118 pg/g tissue) (Fig. 3A). However, there were no statistically significant differences in the mRNA expression levels of IL-6, IP-10, and TNFα in the lung tissues of infected hamsters treated with the extracts (Fig. 3B). Nevertheless, IL-6 and IP-10 levels showed a decreasing trend (~1 log2 reduction) in the *A. paniculata* extract-treated group (Fig. 3B). These findings indicate that *A. paniculata* extract effectively decreases IL-6 levels in the lungs of hamsters infected with the Delta variant of SARS-CoV-2.

3.5. Administration of therapeutic *A. paniculata* or *B. rotunda* extracts significantly reduces IL-6 and IP-10 mRNA expression in the peripheral blood mononuclear cells of infected hamsters

As previously mentioned, higher levels of andrographolide or panduratin A were observed in the blood compared with the lung tissues of hamsters administered with the extracts in this study. This observation prompted us to investigate the potential anti-inflammatory effects of these extracts at the systemic level. To assess this, we examined the expression levels of inflammatory cytokines in PBMCs isolated from the infected hamsters. Total RNA was extracted from the isolated PBMCs, and RT-qPCR was conducted to evaluate the mRNA expression of three selected cytokines (IL-6, IP-10, and TNFα). The comparative CT (ΔΔCT) method was used to calculate the relative expression levels, which were then normalized to β-actin mRNA and presented as relative expression levels compared to the vehicle control group. The results showed a significant reduction in IL-6 and IP-10 mRNA expression levels in the PBMCs of infected hamsters following treatment with both *A. paniculata* and *B. rotunda* extracts (Fig. 4, our findings offer supporting evidence that treatment with *A. paniculata* or *B. rotunda* extract significantly reduces IL-6 and IP-10 mRNA expression levels in PBMCs, indicating their potential as anti-inflammatory agents that can suppress systemic inflammation.

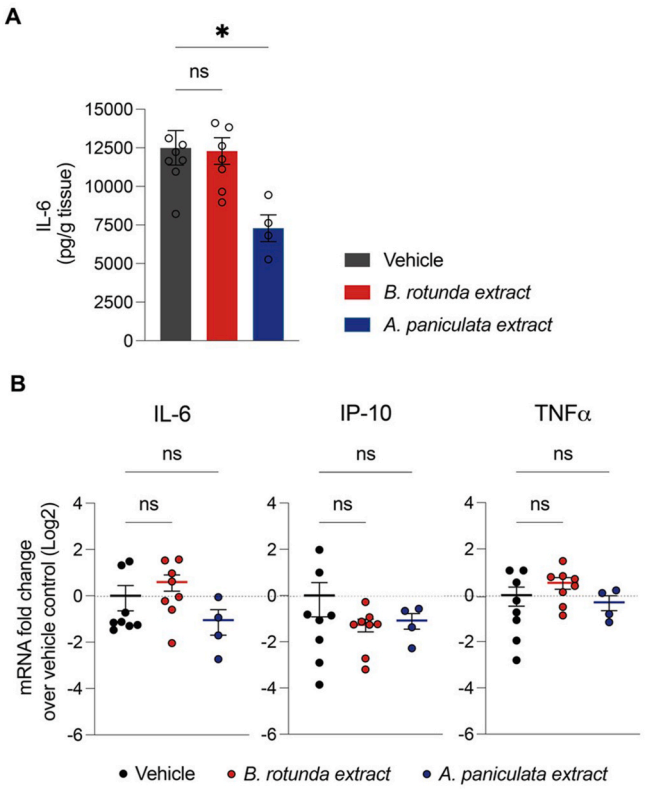

Fig. 3. Effect of *B. rotunda* and *A. paniculata* extracts on protein levels of interleukin 6 (IL-6) and cytokine expression levels in the lung tissue of infected hamsters. Lung tissues of SARS-CoV-2 infected hamsters in vehicle control, *B. rotunda* extract, and *A. paniculata* extract treated group were collected at 3 d.p.i. (A) IL-6 concentration (pg/g tissue) were measured in the RIPA inactivated lung homogenates using ELISA for IL-6 level. (B) mRNA cytokine expression of IL-6, IP-10 and TNF-α in lung tissues were quantified by qRT-PCR and calculated as mRNA fold change over the vehicle control using comparative CT (ΔΔCT) method. Data are presented as mean ± SEM from 4 to 8 hamster per group. Each dot represents individual hamster. Statistical analysis was performed by using non-parametric Kruskal-Wallis test with Dunn's multiple testing. *p < 0.05, ns, not significant.

3.6. Therapeutic *A. paniculata* extract reduces histopathological lesions in the lungs of infected hamsters

We further investigated the efficacy of the extracts in reducing lung damage and thereby improving respiratory function and reducing the severity of SARS-CoV-2-Delta-induced lung symptoms in hamsters. Lung tissue samples were obtained from infected hamsters treated with vehicle, *B. rotunda* extract, or *A. paniculata* extract at 3 d.p.i. H&E staining was performed on the lung tissue sections, and two certified veterinary pathologists independently evaluated the histological changes using the ALI scoring system.[65] The lung histopathology of the hamsters infected with SARS-CoV-2 and treated with vehicle control exhibited extensive lung abnormalities, including necrosis of the bronchial epithelial cells, proteinaceous exudate or cellular debris in the alveoli, alveolar hemorrhaging, thickening of the alveolar septa due to inflammatory cell infiltration, and hyperplasia of the pneumocytes (Fig. 5A–D). Similar lung lesions were observed in the *B. rotunda* extract-treated group (Fig. 5E–H). In contrast, hamsters treated with *A. paniculata* extract showed less severe lung histological changes compared to the vehicle control group. The *A. paniculata* extract-treated group showed no evidence of septal thickening, and the most prominent lesions observed were mild alveolar hemorrhaging and hyperemia (Fig. 5I-L). ALI scores, used to evaluate lung injury, were found to be associated with histological lung damage (Fig. 5M). Notably, hamsters

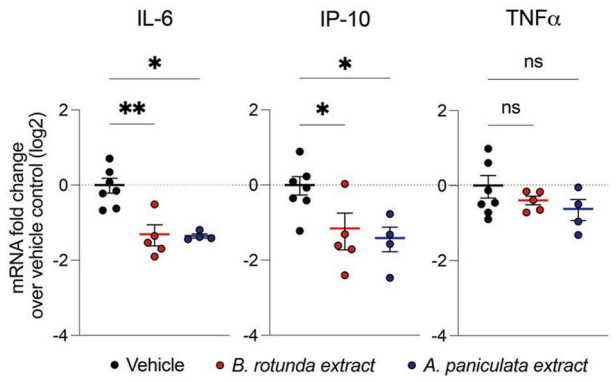

Fig. 4. Effect of *B. rotunda* or *A. paniculata* extracts on cytokine expression levels in PBMCs infected hamsters. Peripheral blood mononuclear cells (PBMCs) were isolated from infected hamsters. Total RNAs were extracted from these cells, and the mRNA cytokine expression levels of IL-6, IP-10, and TNF-α in PBMCs were quantified using qRT-PCR. The cytokine expression levels were calculated as mRNA fold change over the vehicle control group using the comparative CT (ΔΔCT) method. Data are presented as mean ± SEM from 4 to 8 hamster per group. Dot represents individual hamster. Statistical analysis was performed by using non-parametric Kruskal-Wallis test with Dunn's multiple testing. *p < 0.05, **p < 0.01, ns, not significant.

treated with *A. paniculata* extract, but not *B. rotunda* extract, showed a statistically significant reduction in ALI score compared with the vehicle control, indicating the *A. paniculata* extract reduced lung pathology. These results suggested that *A. paniculata* extract may alleviate the severity of SARS-CoV-2 infection by reducing inflammatory cytokine production and lung pathology through its immunomodulatory activity.

3.7. Andrographolide exhibits dose-dependent antiviral activity in SARS-CoV-2 infection in ACE2-TMPRSS2-overexpressing A549 cells with various variants of concern

The emergence of novel variants of SARS-CoV-2 has raised concerns regarding the need for broad antiviral treatments. Previous research has shown the potential of using andrographolide as a monotherapy against SARS-CoV-2 in cell cultures. However, our *in vivo* study showed it had limited antiviral activity in lung tissue, suggesting the poor penetration of andrographolide into the primary site of infection. Enhancing the delivery system could potentially improve andrographolide's distribution in the lungs and increase its antiviral efficacy. This would open up the possibility that andrographolide could be developed as an independent therapeutic agent. We further assessed the *in vitro* anti-viral effect of andrographolide against different SARS-CoV-2 variants, including the omicron variant in ACE2-TMPRSS2-expressing A549 cells. The results showed that andrographolide significantly inhibited the viral replication of all variants of concern (VOC), as evidenced by the dose-dependent decrease in viral nucleoprotein in infected cells (Fig. 6A and B). The IC_{50} calculated for andrographolide were 7.085 μM, 7.354 μM, and 4.619 μM for Alpha, Delta, and Omicron BA.2 variants, respectively (Fig. 6C). These results highlight andrographolide's effectiveness against multiple SARS-CoV-2 variants in lung epithelial cells, emphasizing its potential as a broad-spectrum antiviral for this virus.

4. Discussion

COVID-19 vaccines have reduced the pandemic's impact, generally causing mild symptoms in vaccinated individuals.[69] However, breakthrough infections and resistant strains still pose risks,[9,70] highlighting the need for novel antiviral drugs. Exploring traditional herbal medicines has become a key alternative for resource-limited regions. Recent studies show that herbal compounds effectively inhibit SARS-CoV-2 replication through various mechanisms.[71–73] For instance, *Artemisia*

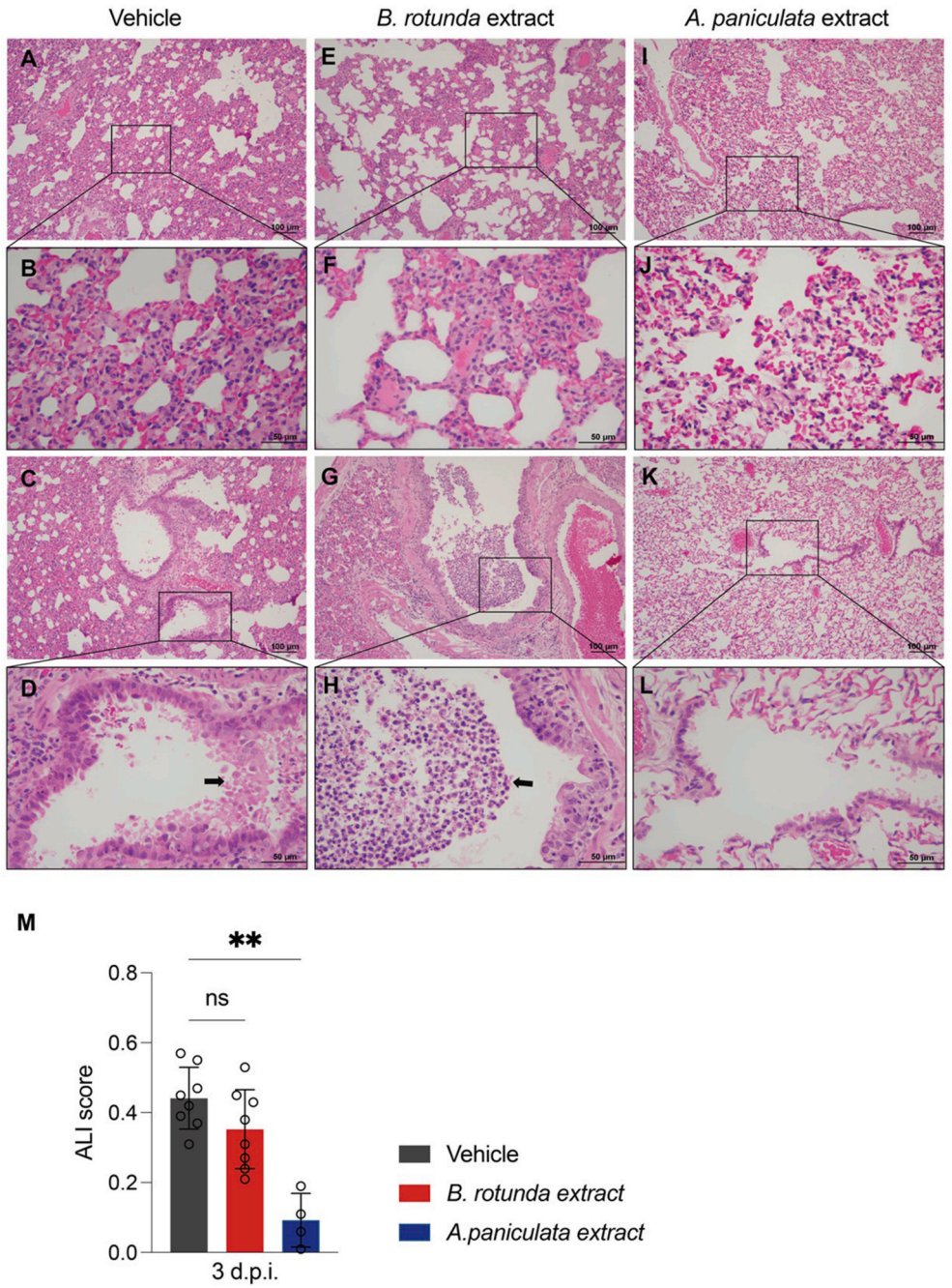

Fig. 5. Histopathological analysis of lung tissue from SARS-CoV-2 infected hamsters treated with *B. rotunda* or *A. paniculata* extracts. Lung tissue of SARS-CoV-2-infected hamsters treated with vehicle, *B. rotunda* extract, and *A. paniculata* extract were collected at 3 days post infection (d.p.i.). The lung tissue sections were then stained with H&E. The representative images of histopathological changes in the lung section were examined (A–P). In the vehicle control group, the lung tissues show thickened alveolar septa combined with inflammatory cell infiltration and hyperplasia of pneumocyte type II (A, 10x and B, 40x), and demonstrate detachment and necrosis of bronchiolar epithelium, accumulation of cellular debris (black arrow, D), inflammatory cells and small number of RBCs in bronchiolar lumen (C, 10x and D, 40x). In *B. rotunda* extract treated group, the lung tissues demonstrate remarkably thickened alveolar septa due to infiltration of inflammatory cells into the septa, and type II pneumocyte hyperplasia (E, 10x and F, 40x), The accumulation of degenerate neutrophils in bronchiolar lumen (black arrow, H) and thickening of mucosal epithelium due to proliferation of bronchiolar epithelial cells infiltration of inflammatory cells into lamina propria (G, 10x and H, 40x). In the *A. paniculata* extract treated group, the lung sections exhibit normal thickness of alveolar septa with mild hyperemia (I, 10x and J, 40x) clear bronchiolar lumen, none of inflammatory cells was detected in the lumen. Only few cellular debris was detected (K, 10x and L, 40x). The histological features of the lung lesion were scored using acute lung injury (ALI) scoring system of an American Thoracic Society (M). Data are presented as mean ± SEM from 4 to 8 hamster per group. Dot represents individual hamster. Statistical analysis was performed by using non-parametric Kruskal-Wallis test with Dunn's multiple testing. **$p < 0.01$, ns, not significant.

annua disrupts viral spike protein and main protease activities, critical for viral replication.[74] Similarly, flavonoids like quercetin and kaempferol from *Ginkgo biloba* block viral entry.[75] Curcumin from *Curcuma longa* prevents viral binding to ACE2 receptors and reduces proinflammatory cytokines, mitigating severe COVID-19 symptoms.[76,77] Additionally, compounds from *Zingiber officinale* provide anti-inflammatory benefits and enhance immune responses.[78] In our previous *in vitro* study, we screened 100 Thai medicinal plants and identified two plants, *A. paniculata* and *B. rotunda*, exhibiting significant anti-SARS-CoV-2 activity at pharmacokinetically achievable

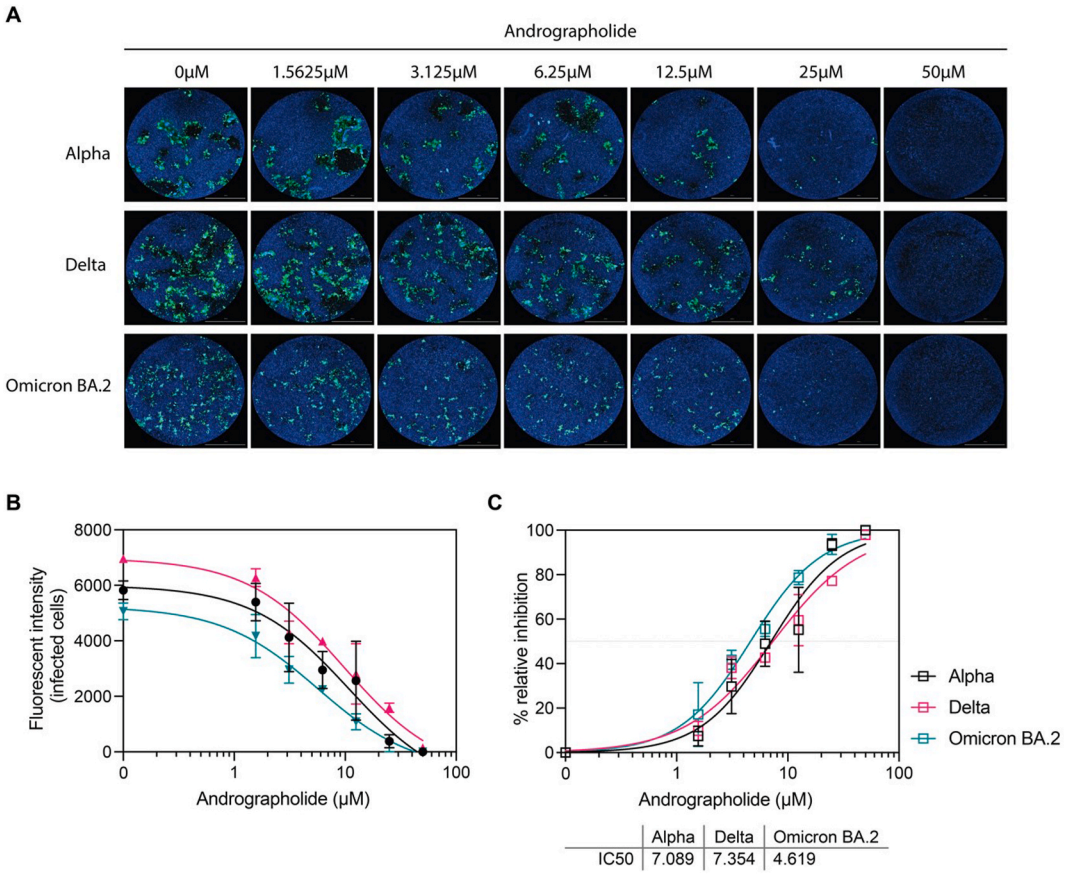

Fig. 6. Antiviral activity of andrographolide upon infection of ACE2TMPRSS2 over expressing A549 cells with different SARS-CoV-2 VOCs. A monolayer of ACE2-TMPRSS2 overexpressing A549 cells infected with different SARS-CoV-2 VOCs (Alpha, Delta, and Omicron) at 25TCID50 and treated with different dosages of andrographolide ranging from 1.56 to 50 μM for 2 days. The infected cells were fixed and stained for viral nucleoproteins. (A) The representative of fluorescent images of SARS-CoV-2 infected cells. Scale bar, 2 mm. The fluorescent intensity of SARS-CoV-2 nucleoprotein-positive cells were measured. (B) Dose-response curve by fluorescent intensity were analyzed. (C) Inhibition of SARS-CoV-2 infection (%) over andrographolide were plotted and IC_{50} were calculated. (n = 2 biological replicates).

concentrations.[14,15] Subsequently, we conducted an *in vivo* efficacy test using hamsters infected with the Wuhan strain of SARS-CoV-2, demonstrating that *B. rotunda* extract protected the infected hamsters from mortality and significantly reduced lung injury.[21] Expanding upon our promising findings, we conducted a comparative study to assess the *in vivo* efficacy of *A. paniculata* and *B. rotunda* against the Delta variant, representing a highly virulent strain of SARS-CoV-2. Our objective was to assess these extracts' antiviral properties and their capacity to reduce inflammation in Golden Syrian hamsters infected with this variant. Infected hamsters treated with *A. paniculata* extract showed significantly lower clinical scores and no severe symptoms or weight loss, leading to a 100 % survival rate, unlike the *B. rotunda* or control groups (Fig. 1B–D).

Our study provides a rationale for exploring immunomodulatory phytotherapeutics like *A. paniculata* as adjunctive treatments for COVID-19. By regulating aberrant inflammation, a key driver of pathogenesis, such approaches could complement direct-acting antivirals in an integrative management strategy for severe cases. Notably, while *A. paniculata* extract did not exhibit direct antiviral effects *in vivo* by reducing lung viral loads (Fig. 2A–C), its therapeutic benefits likely stem from modulating the dysregulated inflammatory response. Despite achieving effective *in vitro* concentrations (Table 1), the limited *in vivo* antiviral activity could be attributed to factors like poor bioavailability, metabolic instability, and protein binding of the bioactive compound andrographolide.[22–27,79,80] Formulation strategies employing drug delivery systems have shown promise in improving andrographolide's pharmacokinetic profile.[81,82] Considering these challenges, future animal studies should prioritize enhancing *in vivo* antiviral efficacy through optimized bioavailability.

In contrast to its lack of direct antiviral effects, *A. paniculata* extract significantly reduced IL-6 protein levels in hamster lung tissue (Fig. 3A), aligning with andrographolide's reported ability to inhibit IL-6 production by targeting several pathways.[28–30,83–86] It inhibits the NF-κB pathway by covalently binding to p50-NF-κB and preventing and phosphorylation of NF-κB related proteins, blocking cytokine production such as IL-6 [83]. Andrographolide also impedes the MAPK signaling pathway by blocking the phosphorylation of ERK1/2, p38, and JNK, crucial in activating AP-1 and HIF-1α.[28–30] Additionally, it targets p-STAT3 in the JAK/STAT pathway to inhibit IL-6 production[84,85] and also interacts with the Nrf2/Keap1 pathway,[83] enhancing the transcription of anti-inflammatory genes, presenting a significant potential for treating inflammation-related conditions. While IL-6, IP-10, and TNF-α mRNA levels were not significantly impacted (Fig. 3B), likely due to post-transcriptional mechanisms, the extract did reduce IL-6 and IP-10 mRNA in peripheral blood mononuclear cells (Fig. 4), corroborating its systemic anti-inflammatory potential.[28,29,87–89] Histopathological analyses further revealed mitigation of lung lesions by *A. paniculata* treatment (Fig. 5). Collectively, these findings suggest *A. paniculata* alleviates COVID-19 severity by modulating inflammatory cytokine production and lung pathology through its immunomodulatory activities.

The contrasting results observed with *B. rotunda* extract, which lacked efficacy in reducing lung viral loads, inflammatory markers, and pathology scores in Delta-infected hamsters, could be attributed to variant-specific differences in inflammatory responses and

pathogenicity.[21,90] Determining optimal dosing regimens tailored to specific SARS-CoV-2 variants may be crucial for realizing *B. rotunda*'s therapeutic potential.

While our study did not include approved antivirals as comparators,[4,5] the findings provide a compelling basis for evaluating phytotherapeutic-antiviral combination regimens. Leveraging the synergistic effects of complementary mechanisms could yield more effective therapeutic strategies against severe COVID-19.

Moreover, our *in vitro* data demonstrating andrographolide's inhibitory activity against emerging Omicron subvariants highlight its potential as a broad-spectrum antiviral candidate. Mechanistic studies have predicted andrographolide may target viral proteins involved in the autophagy-lysosomal pathway, a critical SARS-CoV-2 replication route.[91–93] Exploring these mechanisms could facilitate the way for developing andrographolide derivatives with optimized antiviral potency and drug-like properties.

In summary, our findings underscore the therapeutic promise of *A. paniculata* extract, particularly its principal bioactive andrographolide, as an immunomodulatory and potential broad-spectrum antiviral agent against SARS-CoV-2. Further research delineating its specific anti-inflammatory pathways, evaluating synergies with antivirals, and optimizing its pharmacological properties is warranted to fully harness its potential in an integrative treatment approach for COVID-19.

5. Conclusion

The potential efficacy of *A. paniculata* extract as an adjunct therapeutic intervention for SARS-CoV-2 is derived from its demonstrated ability to reduce levels of inflammatory cytokines and alleviate lung pathology that is linked to viral infection.

Disclaimer

Material has been reviewed by the Walter Reed Army Institute of Research. There is no objection to its presentation and/or publication. The opinions or assertions contained herein are the private views of the authors, and are not to be construed as official, or as reflecting true views of the Department of the Army or the Department of Defense. Research was conducted under an approved animal use protocol in an AAALAC International accredited facility in compliance with the Animal Welfare Act and other federal statutes and regulations relating to animals and experiments involving animals and adheres to principles stated in the Guide for the Care and Use of Laboratory Animals, NRC Publication, 2011 edition.

Declaration of competing interest

The authors declare that they have no known competing financial interests or personal relationships that could have appeared to influence the work reported in this paper.

Acknowledgments

This research project was financially supported by Program Management Unit Competitiveness (PMUC, Grant No. C17F640237) and the Chao Phya Abhaibhubejhr Hospital Foundation. The graphical abstract and Fig. 2A were created with BioRender.com.

We thank Suzanne Leech, Ph.D., from Edanz (www.edanz.com/ac) for editing a draft of this manuscript.

Appendix A. Supplementary data

Supplementary data to this article can be found online at https://doi.org/10.1016/j.jtcme.2024.05.004.

References

1. Dhama K, Khan S, Tiwari R, et al. Coronavirus disease 2019-COVID-19. *Clin Microbiol Rev*. 2020;33(4).
2. Mohammed I, Nauman A, Paul P, et al. The efficacy and effectiveness of the COVID-19 vaccines in reducing infection, severity, hospitalization, and mortality: a systematic review. *Hum Vaccines Immunother*. 2022;18(1), 2027160.
3. Gong W, Parkkila S, Wu X, Aspatwar A. SARS-CoV-2 variants and COVID-19 vaccines: current challenges and future strategies. *Int Rev Immunol*. 2023;42(6):393–414.
4. Vangeel L, Chiu W, De Jonghe S, et al. Remdesivir, Molnupiravir and Nirmatrelvir remain active against SARS-CoV-2 Omicron and other variants of concern. *Antivir Res*. 2022;198, 105252.
5. Rahmah L, Abarikwu SO, Arero AG, et al. Oral antiviral treatments for COVID-19: opportunities and challenges. *Pharmacol Rep*. 2022;74(6):1255–1278.
6. Health NIo. *COVID-19 Treatment Guidelines Panel. Coronavirus Disease 2019 (COVID-19) Treatment Guidelines*. National Institutes of Health; 2020:2020.
7. van de Veerdonk FL, Giamarellos-Bourboulis E, Pickkers P, et al. A guide to immunotherapy for COVID-19. *Nat Med*. 2022;28(1):39–50.
8. Alijotas-Reig J, Esteve-Valverde E, Belizna C, et al. Immunomodulatory therapy for the management of severe COVID-19. Beyond the anti-viral therapy: a comprehensive review. *Autoimmun Rev*. 2020;19(7), 102569.
9. Szemiel AM, Merits A, Orton RJ, et al. In vitro selection of Remdesivir resistance suggests evolutionary predictability of SARS-CoV-2. *PLoS Pathog*. 2021;17(9), e1009929.
10. Badreldin HA, Atallah B. Global drug shortages due to COVID-19: impact on patient care and mitigation strategies. *Res Soc Adm Pharm*. 2021;17(1):1946–1949.
11. Boro E, Stoll B. Barriers to COVID-19 health products in low-and middle-income countries during the COVID-19 pandemic: a rapid systematic review and evidence synthesis. *Front Public Health*. 2022;10, 928065.
12. Wachtel-Galor S, Benzie IFF. Herbal medicine: an introduction to its history, usage, regulation, current trends, and research needs. In: Benzie IFF, Wachtel-Galor S, eds. *Herbal Medicine: Biomolecular and Clinical Aspects*. Boca Raton (FL): CRC Press/Taylor & Francis; 2011.
13. Cai FF, Zhou WJ, Wu R, Su SB. Systems biology approaches in the study of Chinese herbal formulae. *Chin Med*. 2018;13:65.
14. Sa-Ngiamsuntorn K, Suksatu A, Pewkliang Y, et al. Anti-SARS-CoV-2 activity of Andrographis paniculata extract and its major component andrographolide in human lung epithelial cells and cytotoxicity evaluation in major organ cell representatives. *J Nat Prod*. 2021;84(4):1261–1270.
15. Kanjanasirirat P, Suksatu A, Manopwisedjaroen S, et al. High-content screening of Thai medicinal plants reveals Boesenbergia rotunda extract and its component Panduratin A as anti-SARS-CoV-2 agents. *Sci Rep*. 2020;10(1), 19963.
16. Eng-Chong T, Yean-Kee L, Chin-Fei C, et al. Boesenbergia rotunda: from ethnomedicine to drug discovery. *Evid Based Complement Alternat Med*. 2012;2012, 473637.
17. Rukayadi Y, Lee K, Han S, Yong D, Hwang JK. In vitro activities of panduratin A against clinical Staphylococcus strains. *Antimicrob Agents Chemother*. 2009;53(10):4529–4532.
18. Udomthanadech K, Vajrodaya S, Paisooksantivatana Y. Antibacterial properties of the extracts from some Zingibereous species in Thailand against bacteria causing diarrhea and food poisoning in human. *Int Trans J Eng Manag Appl Sci Technol*. 2015;6(5):203–213.
19. Wu N, Kong Y, Zu Y, et al. Activity investigation of pinostrobin towards herpes simplex virus-1 as determined by atomic force microscopy. *Phytomedicine*. 2011;18(2-3):110–118.
20. Isa NM, Abdelwahab SI, Mohan S, et al. In vitro anti-inflammatory, cytotoxic and antioxidant activities of boesenbergin A, a chalcone isolated from Boesenbergia rotunda (L.) (fingerroot). *Braz J Med Biol Res*. 2012;45(6):524–530.
21. Kongratanapasert T, Kongsomros S, Arya N, et al. Pharmacological activities of fingerroot extract and its phytoconstituents against SARS-CoV-2 infection in golden Syrian hamsters. *J Exp Pharmacol*. 2023;15:13–26.
22. Hossain MS, Urbi Z, Sule A, Hafizur Rahman KM, paniculata Andrographis, Burm f. Wall. ex Nees: a review of ethnobotany, phytochemistry, and pharmacology. *Sci World J*. 2014;2014, 274905.
23. Hossain S, Urbi Z, Karuniawati H, et al. Andrographis paniculata (burm. F.) wall. Ex nees: an updated review of phytochemistry, antimicrobial pharmacology, and clinical safety and efficacy. *Life*. 2021;11(4):348.
24. Ding Y, Chen L, Wu W, Yang J, Yang Z, Liu S. Andrographolide inhibits influenza A virus-induced inflammation in a murine model through NF-κB and JAK-STAT signaling pathway. *Microb Infect*. 2017;19(12):605–615.
25. Jayakumar T, Hsieh CY, Lee JJ, Sheu JR. Experimental and clinical pharmacology of Andrographis paniculata and its major bioactive phytoconstituent andrographolide. *Evid Based Complement Alternat Med*. 2013;2013, 846740.
26. Wang J, Tan XF, Nguyen VS, et al. A quantitative chemical proteomics approach to profile the specific cellular targets of andrographolide, a promising anticancer agent that suppresses tumor metastasis. *Mol Cell Proteomics*. 2014;13(3):876–886.
27. Zeng B, Wei A, Zhou Q, et al. Andrographolide: a review of its pharmacology, pharmacokinetics, toxicity and clinical trials and pharmaceutical researches. *Phytother Res*. 2022;36(1):336–364.
28. Kim N, Lertnimitphun P, Jiang Y, et al. Andrographolide inhibits inflammatory responses in LPS-stimulated macrophages and murine acute colitis through activating AMPK. *Biochem Pharmacol*. 2019;170, 113646.
29. Li Y, He S, Tang J, et al. Andrographolide inhibits inflammatory cytokines secretion in LPS-stimulated RAW264.7 cells through suppression of NF-κB/MAPK signaling pathway. *Evid Based Complement Alternat Med*. 2017;2017, 8248142.

30. Nie X, Chen SR, Wang K, et al. Attenuation of innate immunity by andrographolide derivatives through NF-κB signaling pathway. *Sci Rep*. 2017;7(1):4738.
31. Gupta S, Mishra KP, Ganju L. Broad-spectrum antiviral properties of andrographolide. *Arch Virol*. 2017;162(3):611–623.
32. Nutho B, Wilasluck P, Deetanya P, et al. Discovery of C-12 dithiocarbamate andrographolide analogues as inhibitors of SARS-CoV-2 main protease: in vitro and in silico studies. *Comput Struct Biotechnol J*. 2022;20:2784–2797.
33. Shi TH, Huang YL, Chen CC, et al. Andrographolide and its fluorescent derivative inhibit the main proteases of 2019-nCoV and SARS-CoV through covalent linkage. *Biochem Biophys Res Commun*. 2020;533(3):467–473.
34. Patcharanaruamol W, Lekagul A, Akaleephan C, Markchang K, Phaiyarom M, Rajatanavin N. *COVID-19 Health System Response Monitor: Thailand*. New Delhi: World Health Organization Regional Office for South-East Asia; 2020.
35. Tanwettiyanont J, Piriyachananusorn N, Sangsoi L, et al. Use of Andrographis paniculata (Burm.f.) Wall. ex Nees and risk of pneumonia in hospitalised patients with mild coronavirus disease 2019: a retrospective cohort study. *Front Med*. 2022;9, 947373.
36. World Health Organization. *Statement on the Fifteenth Meeting of the IHR (2005) Emergency Committee on the COVID-19 Pandemic*. World Health Organization; 2023.
37. Khateeb J, Li Y, Zhang H. Emerging SARS-CoV-2 variants of concern and potential intervention approaches. *Crit Care*. 2021;25(1):244.
38. Hirabara SM, Serdan TDA, Gorjao R, et al. SARS-COV-2 variants: differences and potential of immune evasion. *Front Cell Infect Microbiol*. 2021;11, 781429.
39. Fan Y, Li X, Zhang L, Wan S, Zhang L, Zhou F. SARS-CoV-2 Omicron variant: recent progress and future perspectives. *Signal Transduct Targeted Ther*. 2022;7(1):141.
40. Chen Z, Azman AS, Chen X, et al. Global landscape of SARS-CoV-2 genomic surveillance and data sharing. *Nat Genet*. 2022;54(4):499–507.
41. Sigal A. Milder disease with Omicron: is it the virus or the pre-existing immunity? *Nat Rev Immunol*. 2022;22(2):69–71.
42. Auvigne V, Vaux S, Strat YL, et al. Severe hospital events following symptomatic infection with Sars-CoV-2 Omicron and Delta variants in France, December 2021-January 2022: a retrospective, population-based, matched cohort study. *EClinicalMedicine*. 2022;48, 101455.
43. Adjei S, Hong K, Molinari NM, et al. Mortality risk among patients hospitalized primarily for COVID-19 during the omicron and Delta variant pandemic periods - United States, April 2020-June 2022. *MMWR Morb Mortal Wkly Rep*. 2022;71(37):1182–1189.
44. Wrenn JO, Pakala SB, Vestal G, et al. COVID-19 severity from Omicron and Delta SARS-CoV-2 variants. *Influenza Other Respir Viruses*. 2022;16(5):832–836.
45. Rajah MM, Hubert M, Bishop E, et al. SARS-CoV-2 Alpha, Beta, and Delta variants display enhanced Spike-mediated syncytia formation. *EMBO J*. 2021;40(24), e108944.
46. Saito A, Irie T, Suzuki R, et al. Enhanced fusogenicity and pathogenicity of SARS-CoV-2 Delta P681R mutation. *Nature*. 2022;602(7896):300–306.
47. Braga L, Ali H, Secco I, et al. Drugs that inhibit TMEM16 proteins block SARS-CoV-2 spike-induced syncytia. *Nature*. 2021;594(7861):88–93.
48. Bussani R, Schneider E, Zentilin L, et al. Persistence of viral RNA, pneumocyte syncytia and thrombosis are hallmarks of advanced COVID-19 pathology. *EBioMedicine*. 2020;61, 103104.
49. Buchrieser J, Dufloo J, Hubert M, et al. Syncytia formation by SARS-CoV-2-infected cells. *EMBO J*. 2020;39(23), e106267.
50. Rajah MM, Bernier A, Buchrieser J, Schwartz O. The mechanism and consequences of SARS-CoV-2 spike-mediated fusion and syncytia formation. *J Mol Biol*. 2022;434(6), 167280.
51. Zhao H, Lu L, Peng Z, et al. SARS-CoV-2 Omicron variant shows less efficient replication and fusion activity when compared with Delta variant in TMPRSS2-expressed cells. *Emerg Microb Infect*. 2022;11(1):277–283.
52. Pia L, Rowland-Jones S. Omicron entry route. *Nat Rev Immunol*. 2022;22(3):144.
53. Meng B, Abdullahi A, Ferreira I, et al. Altered TMPRSS2 usage by SARS-CoV-2 Omicron impacts infectivity and fusogenicity. *Nature*. 2022;603(7902):706–714.
54. Zhang Y, Zhang T, Fang Y, Liu J, Ye Q, Ding L. SARS-CoV-2 spike L452R mutation increases Omicron variant fusogenicity and infectivity as well as host glycolysis. *Signal Transduct Targeted Ther*. 2022;7(1):76.
55. Tamura T, Ito J, Uriu K, et al. Virological characteristics of the SARS-CoV-2 XBB variant derived from recombination of two Omicron subvariants. *Nat Commun*. 2023;14(1):2800.
56. Ragab D, Salah Eldin H, Taeimah M, Khattab R, Salem R. The COVID-19 cytokine storm; what we know so far. *Front Immunol*. 2020;11:1446.
57. de la Rica R, Borges M, Gonzalez-Freire M. COVID-19: in the eye of the cytokine storm. *Front Immunol*. 2020;11, 558898.
58. Fajgenbaum DC, June CH. Cytokine storm. *N Engl J Med*. 2020;383(23):2255–2273.
59. Vacharathit V, Srichatrapimuk S, Manopwisedjaroen S, et al. SARS-CoV-2 neutralizing antibodies decline over one year and patients with severe COVID-19 pneumonia display a unique cytokine profile. *Int J Infect Dis*. 2021;112:227–234.
60. Liu T, Zhang J, Yang Y, et al. The role of interleukin-6 in monitoring severe case of coronavirus disease 2019. *EMBO Mol Med*. 2020;12(7), e12421.
61. Zhang Q, Xiang R, Huo S, et al. Molecular mechanism of interaction between SARS-CoV-2 and host cells and interventional therapy. *Signal Transduct Targeted Ther*. 2021;6(1):233.
62. Chaturvedi S, Beutler N, Vasen G, et al. A single-administration therapeutic interfering particle reduces SARS-CoV-2 viral shedding and pathogenesis in hamsters. *Proc Natl Acad Sci U S A*. 2022;119(39), e2204624119.
63. Sia SF, Yan LM, Chin AWH, et al. Pathogenesis and transmission of SARS-CoV-2 in golden hamsters. *Nature*. 2020;583(7818):834–838.
64. Boudewijns R, Thibaut HJ, Kaptein SJF, et al. STAT2 signaling restricts viral dissemination but drives severe pneumonia in SARS-CoV-2 infected hamsters. *Nat Commun*. 2020;11(1):5838.
65. Matute-Bello G, Downey G, Moore BB, et al. An official American Thoracic Society workshop report: features and measurements of experimental acute lung injury in animals. *Am J Respir Cell Mol Biol*. 2011;44(5):725–738.
66. Zhang X, Chen S, Cao Z, et al. Increased pathogenicity and aerosol transmission for one SARS-CoV-2 B.1.617.2 Delta variant over the wild-type strain in hamsters. *Virol Sin*. 2022;37(6):796–803.
67. Mohandas S, Yadav PD, Shete A, et al. SARS-CoV-2 Delta variant pathogenesis and host response in Syrian hamsters. *Viruses*. 2021;13(9):1773.
68. Lange NR, Schuster DP. The measurement of lung water. *Crit Care*. 1999;3(2):R19–r24.
69. Rahmani K, Shavaleh R, Forouhi M, et al. The effectiveness of COVID-19 vaccines in reducing the incidence, hospitalization, and mortality from COVID-19: a systematic review and meta-analysis. *Front Public Health*. 2022;10, 873596.
70. Lipsitch M, Krammer F, Regev-Yochay G, Lustig Y, Balicer RD. SARS-CoV-2 breakthrough infections in vaccinated individuals: measurement, causes and impact. *Nat Rev Immunol*. 2022;22(1):57–65.
71. Fuzimoto AD, Isidoro C. The antiviral and coronavirus-host protein pathways inhibiting properties of herbs and natural compounds - additional weapons in the fight against the COVID-19 pandemic? *J Tradit Complement Med*. 2020;10(4):405–419.
72. Demeke CA, Woldeyohanins AE, Kifle ZD. Herbal medicine use for the management of COVID-19: a review article. *Metabol Open*. 2021;12, 100141.
73. Liu YX, Zhou YH, Jiang CH, Liu J, Chen DQ. Prevention, treatment and potential mechanism of herbal medicine for Corona viruses: a review. *Bioengineered*. 2022;13(3):5480–5508.
74. Baggieri M, Gioacchini S, Borgonovo G, et al. Antiviral, virucidal and antioxidant properties of Artemisia annua against SARS-CoV-2. *Biomed Pharmacother*. 2023;168, 115682.
75. Khazdair MR, Anaeigoudari A, Agbor GA. Anti-viral and anti-inflammatory effects of kaempferol and quercetin and COVID-2019: a scoping review. *Asian Pac J Trop Biomed*. 2021;11(8):327–334.
76. Patel A, Rajendran M, Shah A, Patel H, Pakala SB, Karyala P. Virtual screening of curcumin and its analogs against the spike surface glycoprotein of SARS-CoV-2 and SARS-CoV. *J Biomol Struct Dyn*. 2022;40(11):5138–5146.
77. Vahedian-Azimi A, Abbasifard M, Rahimi-Bashar F, et al. Effectiveness of curcumin on outcomes of hospitalized COVID-19 patients: a systematic review of clinical trials. *Nutrients*. 2022;14(2):256.
78. Al-Jamal H, Idriss S, Roufayel R, Abi Khattar Z, Fajloun Z, Sabatier JM. Treating COVID-19 with medicinal plants: is it even conceivable? A comprehensive review. *Viruses*. 2024;16(3):320.
79. Longuespée R, Theile D, Fresnais M, Burhenne J, Weiss J, Haefeli WE. Approaching sites of action of drugs in clinical pharmacology: new analytical options and their challenges. *Br J Clin Pharmacol*. 2021;87(3):858–874.
80. Malarvizhi K. Review on the various drug delivery systems of andrographolide. *Phytopharm. Drug Deliv. Approaches*. 2019:2–13.
81. Casamonti M, Risaliti L, Vanti G, Piazzini V, Bergonzi MC, Bilia AR. Andrographolide loaded in micro-and nano-formulations: improved bioavailability, target-tissue distribution, and efficacy of the “king of bitters”. *Engineering*. 2019;5(1):69–75.
82. Songvut P, Boonyarattanasoonthorn T, Nuengchamnong N, et al. Enhancing oral bioavailability of andrographolide using solubilizing agents and bioenhancer: comparative pharmacokinetics of *Andrographis paniculata* formulations in beagle dogs. *Pharm Biol*. 2024;62(1):183–194.
83. Burgos RA, Alarcón P, Quiroga J, Manosalva C, Hancke J. Andrographolide, an anti-inflammatory multitarget drug: all roads lead to cellular metabolism. *Molecules*. 2020;26(1).
84. Chun JY, Tummala R, Nadiminty N, et al. Andrographolide, an herbal medicine, inhibits interleukin-6 expression and suppresses prostate cancer cell growth. *Genes Cancer*. 2010;1(8):868–876.
85. Kou W, Sun R, Wei P, et al. Andrographolide suppresses IL-6/Stat3 signaling in peripheral blood mononuclear cells from patients with chronic rhinosinusitis with nasal polyps. *Inflammation*. 2014;37(5):1738–1743.
86. Li X, Yuan W, Wu J, Zhen J, Sun Q, Yu M. Andrographolide, a natural anti-inflammatory agent: an Update. *Front Pharmacol*. 2022;13, 920435.
87. Guan SP, Tee W, Ng DS, et al. Andrographolide protects against cigarette smoke-induced oxidative lung injury via augmentation of Nrf2 activity. *Br J Pharmacol*. 2013;168(7):1707–1718.
88. He W, Sun J, Zhang Q, et al. Andrographolide exerts anti-inflammatory effects in Mycobacterium tuberculosis-infected macrophages by regulating the Notch1/Akt/NF-κB axis. *J Leukoc Biol*. 2020;108(6):1747–1764.

89. Wong SY, Tan MG, Banks WA, Wong WS, Wong PT, Lai MK. Andrographolide attenuates LPS-stimulated up-regulation of C-C and C-X-C motif chemokines in rodent cortex and primary astrocytes. *J Neuroinflammation*. 2016;13:34.
90. Ao Z, Ouyang MJ, Olukitibi TA, Yao X. SARS-CoV-2 Delta spike protein enhances the viral fusogenicity and inflammatory cytokine production. *iScience*. 2022;25(8), 104759.
91. Ghosh S, Dellibovi-Ragheb TA, Kerviel A, et al. β-Coronaviruses use lysosomes for egress instead of the biosynthetic secretory pathway. *Cell*. 2020;183(6):1520–1535.e1514.
92. Khanal P, Dey YN, Patil R, et al. Combination of system biology to probe the anti-viral activity of andrographolide and its derivative against COVID-19. *RSC Adv*. 2021;11(9):5065–5079.
93. Vidoni C, Fuzimoto A, Ferraresi A, Isidoro C. Targeting autophagy with natural products to prevent SARS-CoV-2 infection. *J Tradit Complement Med*. 2022;12(1):55–68.